Pressure Elucidates Self-Trapped Exciton Emissions and Piezochromism in Hybrid Copper Halide

Yufan Meng[a], Ziniu Yang[a], Jingze Du[a], Xihan Yu[a], Jiayi Yang[a], Ming Cong[*b], Guanjun Xiao[*a], and Bo Zou[a]

a: State Key Laboratory of High Pressure and Superhard Materials, College of Physics, Jilin University, Changchun 130012, China

b: Guangxi Univ Sci & Technol, Sch Sci, Liuzhou 545006, China

Experimental Section

Materials.

Copper(I) bromide (CuBr, 99.0%, Aladdin), tetrabutylammonium bromide (TBABr, 99%, Damas), isopropanol (IPA, ≥99.7%, General-reagent), ethanol (EtOH, ≥99.7%, Sinopharm), and hypophosphorous acid (H_3PO_2, 50 wt% in H_2O, Damas) were used as received without further purification.

Synthesis of $(TBA)_2Cu_4Br_6$ Single Crystals (SCs).

$(TBA)_2Cu_4Br_6$ single crystals were synthesized via a slow cooling method. Typically, TBABr (1 mmol) and CuBr (2 mmol) were dissolved in a mixture of IPA (20 mL) and H_3PO_2 (0.06 mL) under continuous stirring at 100 °C for 3 hours. The resulting hot solution was filtered, and EtOH (5 mL) was promptly added to the filtrate. The mixture was then allowed to cool slowly to room temperature over 6 hours, yielding orange-emitting sheet-like single crystals.

High-Pressure Generation.

High-pressure conditions were generated using a symmetric diamond anvil cell (DAC) with 400 μm culet diamonds. A T301 steel gasket was preindented to a thickness of 45 μm before a 150 μm diameter hole was drilled to act as the sample chamber in the center. The pressure was calibrated using the ruby fluorescence method, with a small ruby sphere placed inside the chamber as a pressure sensor. Finely ground microcrystalline powder of $(TBA)_2Cu_4Br_6$ was loaded into the chamber along with silicone oil as a hydrostatic pressure-transmitting medium. The DAC was then carefully closed to seal the sample chamber. To minimize the pressure hysteresis effect, the system was allowed to stabilize for several minutes at each target pressure before spectral measurements and pressure calibration were performed.

In Situ High-Pressure Optical Characterization.

All steady-state photoluminescence (PL) measurements were conducted using a 355 nm semiconductor laser as the excitation source. The laser beam was attenuated and focused onto the sample through a 20× UV Plan apochromatic objective, yielding a spot size of approximately 20 μm. A suitable filter was used to eliminate stray laser light during signal acquisition. To ensure consistency, all experimental parameters—including laser power and collection geometry—were kept identical throughout the high-pressure PL measurements. Absorption spectra across the excitonic absorption region were acquired using a deuterium-halogen light source. Both PL and absorption spectra were recorded with an optical fiber spectrometer (Ocean Optics QE65000), employing integration times of 300 ms and 500 ms, respectively. High-pressure Raman spectra were collected on a Raman spectrometer (Princeton Instruments SP2500i) equipped with a 532 nm laser operating at 10 mW power and an integration time of 10 s. Additionally, infrared absorption measurements were performed using a Bruker Vertex 70 V FT-IR spectrometer. For time-resolved PL measurements, a 375 nm pulsed diode laser (LDH-P-C-375B, 40 ps pulse width) was used as the excitation source, and the resulting signals were analyzed by a grating spectrometer (HRS-500 MS) coupled with a time-correlated single photon counting unit (TimeHarp 260 PICO).

In Situ High-Pressure X-ray Diffraction Measurements.

Angle-dispersive X-ray diffraction (XRD) experiments under high pressure were conducted at the 15U1 beamline of the Shanghai Synchrotron Radiation Facility (SSRF). A monochromatic X-ray beam with a wavelength of 0.6199 Å was focused to a spot size of approximately 4 × 3.5 μm^2 for the measurements. CeO_2 was used as a standard for diffraction angle calibration. The two-dimensional diffraction patterns were collected using a Mar-165 CCD detector with an exposure time of 10 seconds per pattern, and subsequently integrated into one-dimensional intensity profiles using the Fit2D software.

Data analyses

The Reflex module combined in Materials Studio was applied for Rietveld refinement. The pressure–volume data were analyzed by fitting to the third-order Birch–Murnaghan equation of state[1]:

$$P = \frac{3}{2}B_0 \times [(\frac{V}{V_0})^{-\frac{7}{3}} - (\frac{V}{V_0})^{-\frac{5}{3}}] \times \{1 + \frac{3}{4}(B_0^{'} - 4) \times [(\frac{V}{V_0})^{-\frac{2}{3}} - 1]\} \quad (1)$$

In this equation, V_0 refers to the volume at zero pressure, B_0 is the bulk modulus under ambient pressure, and $B_0^{'}$ is the pressure derivative of the bulk modulus. All high-pressure measurements were conducted at room temperature.

The trigonal variance of distortion in bond length (Δd) based on the following parameters[2]:

$$\Delta d = \frac{1}{3}\Sigma_{i=1}^{3}[(d_i - d_0)/d_0]^2 \quad (2)$$

The time resolved PL decay curves were fitted by the double exponential function[3]:

$$I(t) = I_0 + A_1 \times \exp\left(-\frac{t}{\tau_1}\right) + A_2 \times \exp\left(-\frac{t}{\tau_2}\right) + A_3 \times \exp\left(-\frac{t}{\tau_3}\right) \quad (3)$$

$$\tau_{ave} = \frac{\Sigma\alpha_i \times \tau_i^2}{\Sigma\alpha_i \times \tau_i}, i = 1,2,3 \quad (4)$$

First-principles calculations

First-principles calculations were performed using the plane-wave pseudopotential method within the generalized gradient approximation (GGA) of density functional theory (DFT), as implemented in the CASTEP package. The initial crystal structure was retrieved from the Cambridge Structure Database. A kinetic energy cutoff of 400 eV and a Monkhorst–Pack k-point mesh of 3×2×2 were employed for geometry optimizations. The convergence thresholds were set at values of 1.0 e^{-6} eV/atom for energy and 0.03 $eVÅ^{-1}$ for force.

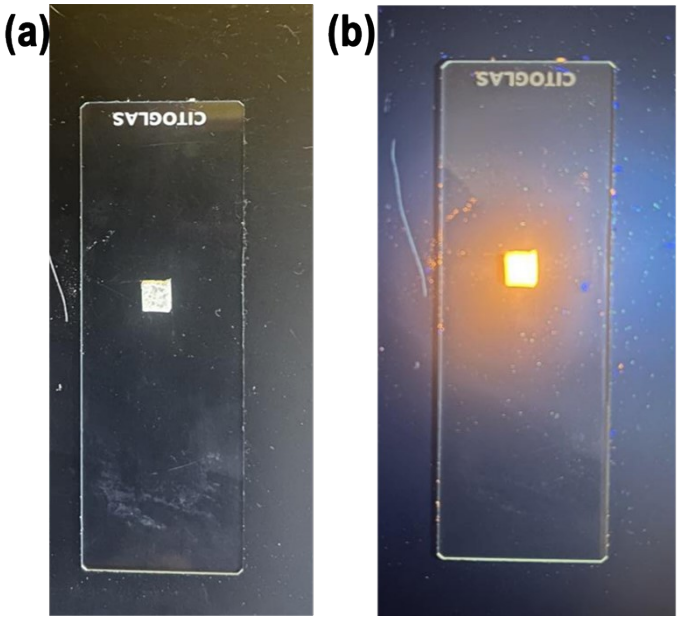

Figure S1. Optical and luminescent images of synthesized $(TBA)_2Cu_4Br_6$ powder. (a) Photograph under ambient light. (b) Photograph under 355 nm UV irradiation.

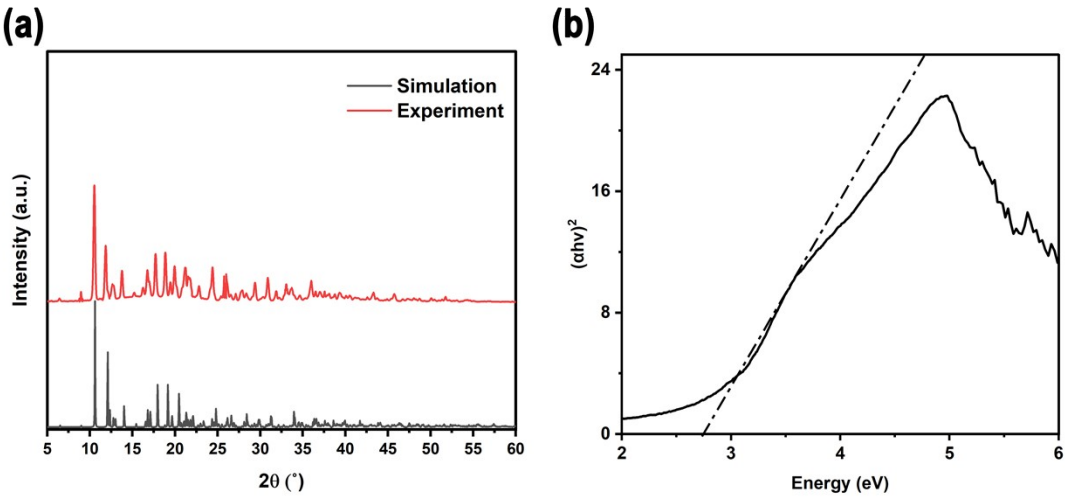

Figure S2. XRD patterns of synthesized $(TBA)_2Cu_4Br_6$ and Tauc-plot analysis. (a) Experimental data compared with the theoretical simulation from Materials Studio. (b) Tauc plot $((\alpha h\nu)^2$ vs. $h\nu)$ for direct bandgap determination at ambient pressure.

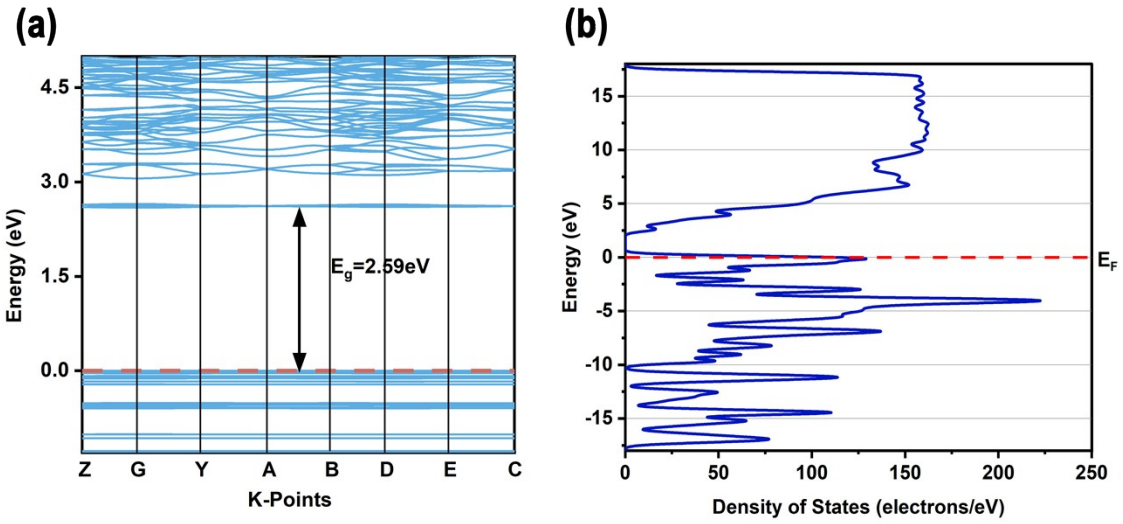

Figure S3. Calculated electronic structure. (a) Electronic band structure and (b) density of states (DOS) of $(TBA)_2Cu_4Br_6$ simulated with Materials Studio.

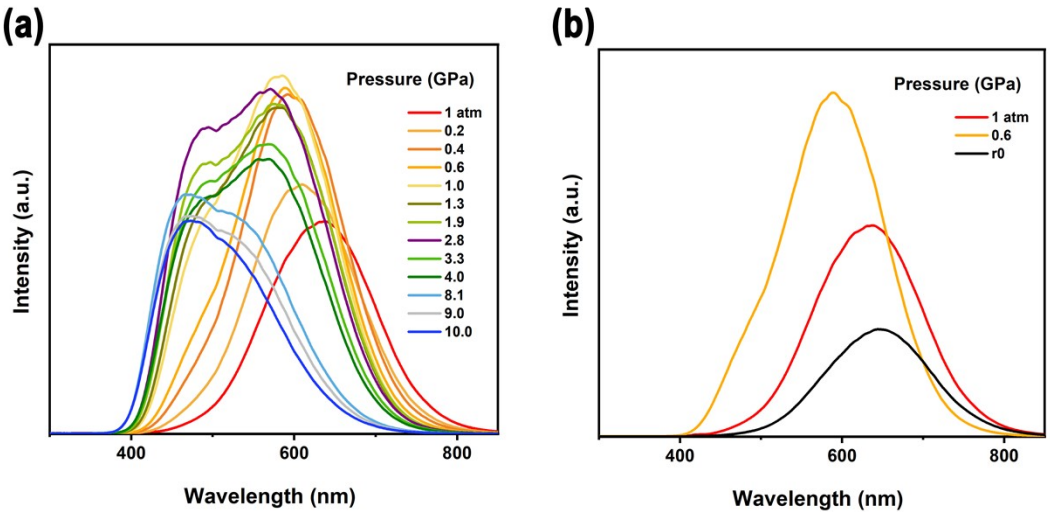

Figure S4. High-pressure photoluminescence spectra. Pressure-dependent PL spectra of $(TBA)_2Cu_4Br_6$ under 355 nm laser excitation.

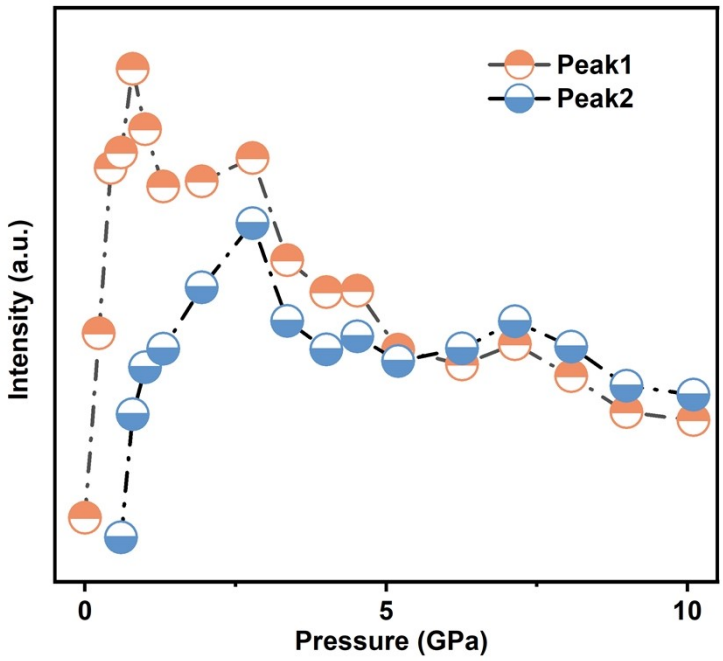

Figure S5. Pressure-dependent emission intensity evolution. Integrated intensities of Peak 1 (triplet STEs) and Peak 2 (singlet STEs) for $(TBA)_2Cu_4Br_6$ as a function of pressure.

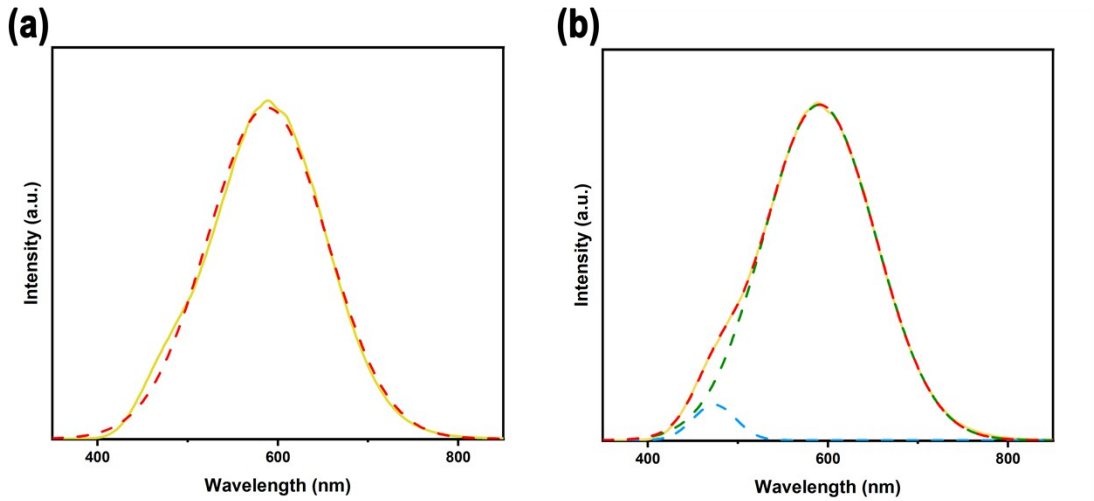

Figure S6. Spectral Fitting at the Phase Transition Pressure. Unimodal and bimodal fitting of the photoluminescence spectrum for $(TBA)_2Cu_4Br_6$ at 0.6 GPa.

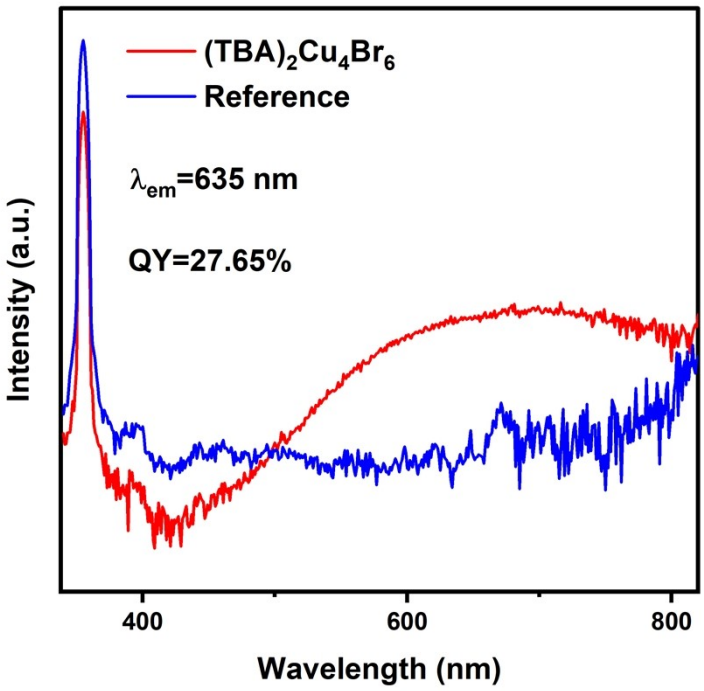

Figure S7. Photoluminescence quantum yield. PLQY measurement of $(TBA)_2Cu_4Br_6$ at ambient conditions.

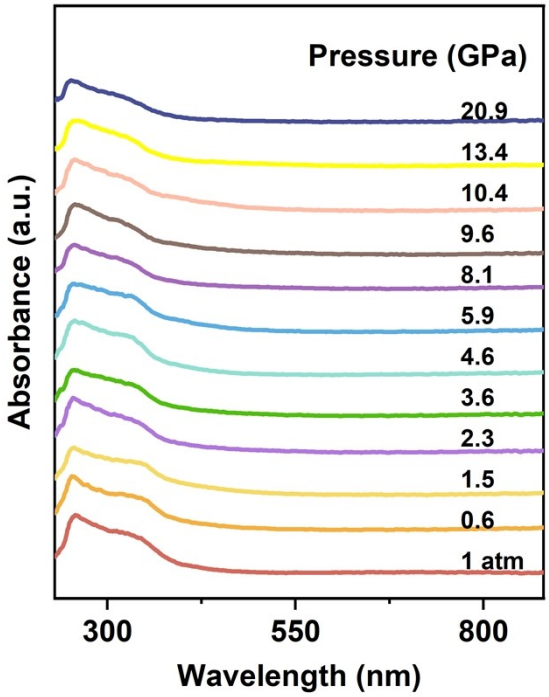

Figure S8. High-pressure absorption. Pressure-dependent UV-Vis absorption spectra.

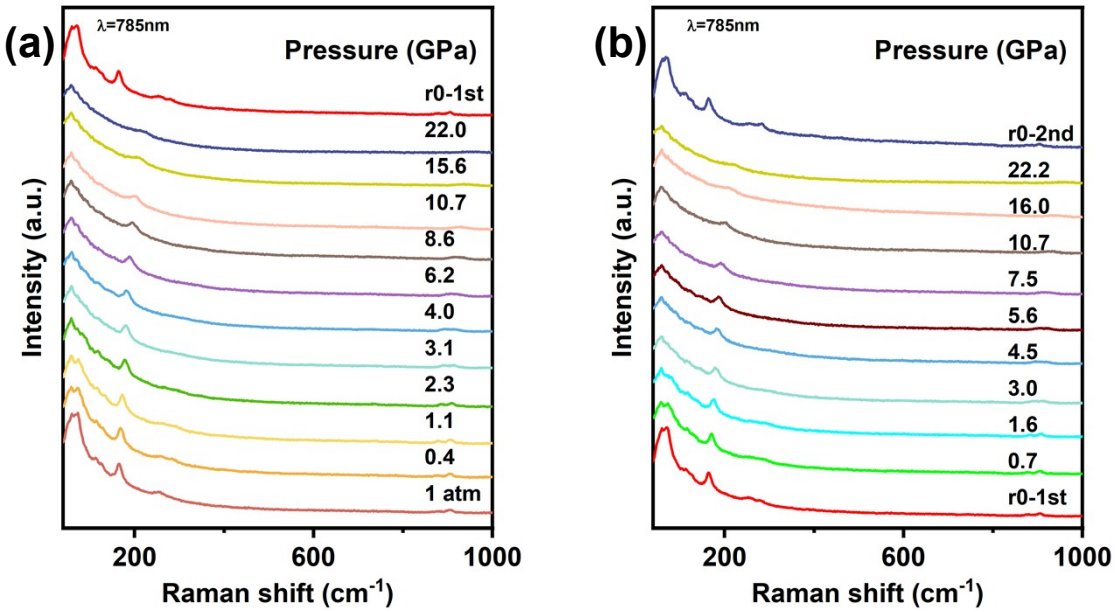

Figure S9. High-pressure Raman spectra of $(TBA)_2Cu_4Br_6$ over two consecutive compression-decompression cycles. (a) First compression and decompression. (b) Second compression and decompression.

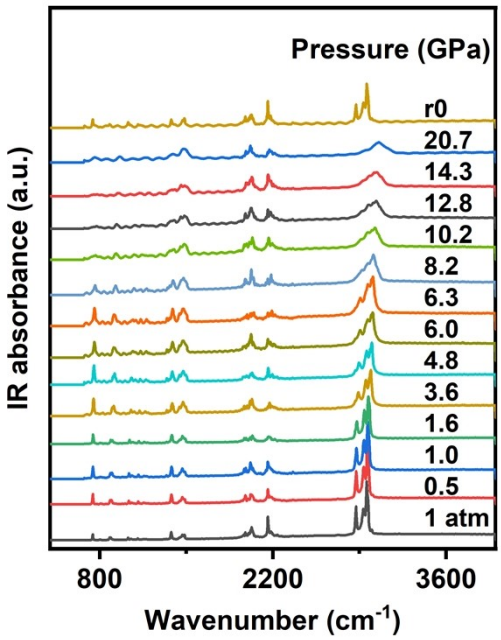

Figure S10. High-pressure FTIR spectra. Pressure-dependent evolution of Fourier-transform infrared (FTIR) spectra for $(TBA)_2Cu_4Br_6$.

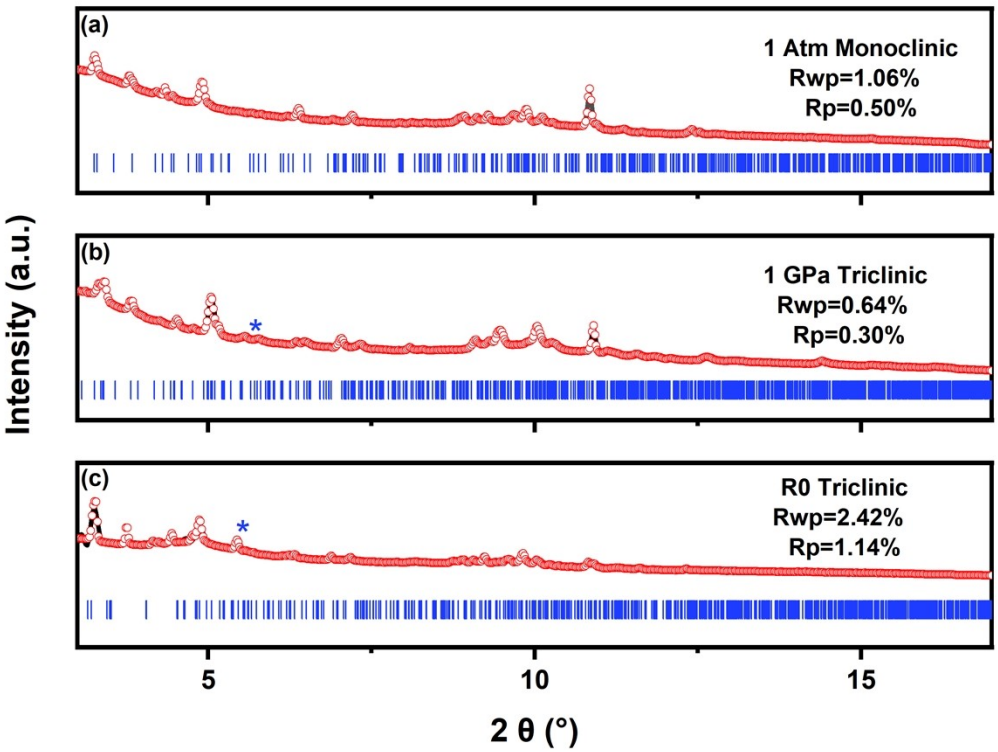

Figure S11. Rietveld refinement of synchrotron XRD data. Rietveld refinement profiles for $(TBA)_2Cu_4Br_6$ at (a) 1 atm, (b) 1 GPa, (c) R0, release to 1 atm

Table S1. Refinement cell parameters and refinement statistics at 1 atm, 1.0 GPa and R0.

Pressure (GPa)	**1 atm**	**1.0 GPa**	**R0**
Temperature (K)	293	293	293
Crystal system	Monoclinic	Triclinic	Triclinic
Space group	$P2_1/n$	P-1	P-1
a (Å)	16.4374	15.9404	16.0234
b (Å)	16.0105	15.5159	15.9079
c (Å)	20.1525	19.354	20.0656
α (°)	90	88.814	88.9815
β (°)	111.998	110.401	110.989
γ (°)	90	88.804	89.0105
Volume (Å^3)	4917.41	4483.62	4773.08
θ range (°)	3-17	3-17	3-17
Wavelength (Å)	0.6199	0.6199	0.6199
R_{wp} (%)	1.06	0.64	2.30
R_p(%)	0.5	0.3	1.06

Table S2. Evolution of Cu-Cu bond lengths with pressure.

Pressure (GPa)	Cu-Cu Distance (Å)						
	Cu_1-Cu_2	Cu_2-Cu_3	Cu_2-Cu_4	Cu_3-Cu_4	Cu_1-Cu_3	Cu1-Cu_4	Average
1 atm	2.77722	2.74474	2.72825	2.78093	2.71268	2.74798	2.74863
1	2.71239	2.64339	2.6259	2.63987	2.63652	2.66891	2.6545
2.2	2.61784	2.4832	2.46204	2.48917	2.50282	2.56408	2.51986
3	2.60246	2.46486	2.44622	2.47323	2.48796	2.54598	2.50345
4	2.59276	2.45403	2.42739	2.47221	2.46703	2.54686	2.49338
5	2.58091	2.44184	2.41713	2.46017	2.45443	2.53334	2.4813
6	2.56494	2.42394	2.40327	2.44316	2.43575	2.5143	2.46423
7.2	2.5636	2.41891	2.40425	2.43867	2.4303	2.50762	2.46056
8.1	2.5376	2.39836	2.3943	2.40161	2.42685	2.46716	2.43765
10	2.51941	2.38464	2.37989	2.38295	2.41856	2.4486	2.42234

Table S3. Evolution of Cu-Br bond lengths with pressure.

Pressure (GPa)		1 atm	1	2.2	3	4	5	6	7.2	8.1	10
Cu-Br Distance (Å)	Cu_1-Br_1	2.39622	2.28532	2.14921	2.1361	2.12746	2.1181	2.10544	2.10494	2.0841	2.06899
	Cu_1-Br_5	2.40388	2.32559	2.17871	2.16319	2.14609	2.13635	2.12251	2.12124	2.11418	2.10323
	Cu_1-Br_6	2.40147	2.29135	2.15905	2.14382	2.14227	2.13126	2.11512	2.10937	2.07919	2.06471
	Cu_2-Br_2	2.40834	2.30514	2.19757	2.18214	2.18798	2.17681	2.16132	2.15638	2.11278	2.09372
	Cu_2-Br_3	2.3939	2.29089	2.15578	2.14316	2.12985	2.11946	2.10422	2.10034	2.08905	2.07898
	Cu_2-Br_5	2.39301	2.34309	2.24542	2.23074	2.21884	2.20704	2.18985	2.18403	2.16986	2.15981
	Cu_3-Br_3	2.37663	2.30379	2.18704	2.17437	2.15786	2.14901	2.13732	2.13901	2.12965	2.11616
	Cu_3-Br_4	2.41197	2.32598	2.19717	2.18152	2.17434	2.16362	2.1486	2.1452	2.12242	2.1084
	Cu_3-Br_6	2.39868	2.34515	2.27665	2.26195	2.26189	2.25028	2.2342	2.22946	2.19461	2.17764
	Cu_4-Br_1	2.37207	2.32017	2.23561	2.22345	2.20934	2.19881	2.18415	2.18185	2.17	2.15836
	Cu_4-Br_2	2.39823	2.3258	2.22031	2.20533	2.19953	2.18933	2.17528	2.17331	2.14742	2.13129
	Cu_4-Br_4	2.4158	2.33092	2.18457	2.1695	2.15284	2.14159	2.1245	2.11856	2.11321	2.10596

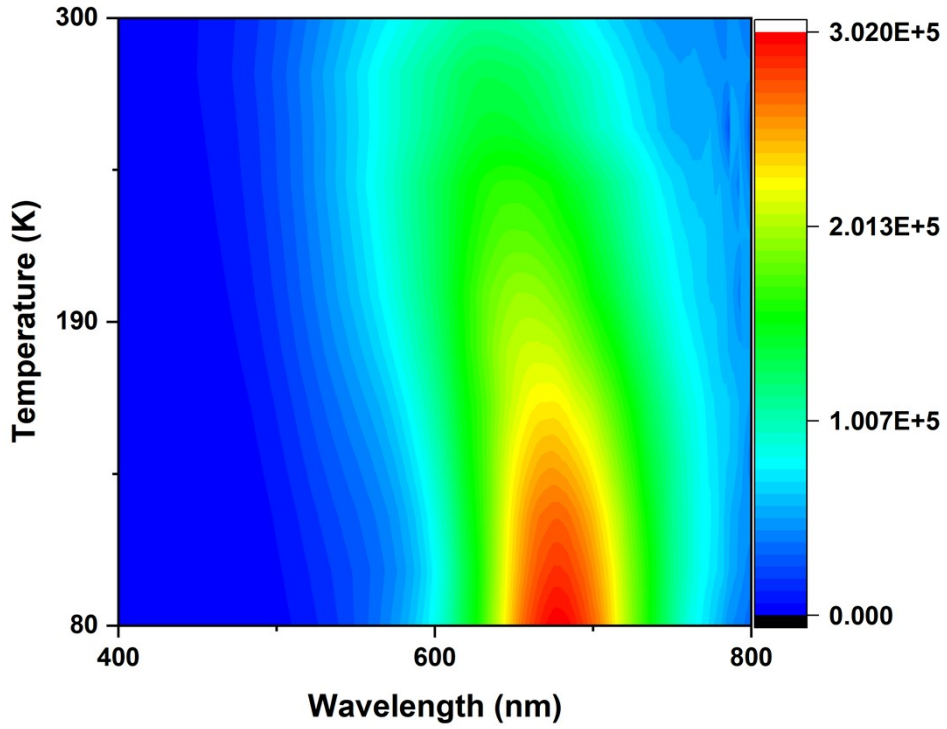

Figure S12. Temperature-dependent PL spectra of $(TBA)_2Cu_4Br_6$ from 80 to 300 K. Contour mapping of PL emission spectra as a function of temperature.

Table S4. Excitation energies and dominant orbital contributions of the excited states at selected pressures.

Pressure	State	Singlet		Triplet	
		Exc. Energy (eV)	MO pairs	Exc. Energy (eV)	MO pairs
1 atm	1	2.699	9	2.565	35
	2	2.7	8	2.565	36
	3	2.703	12	2.566	36
	4	2.704	8	2.566	35
	5	2.707	9	2.574	29
	6	2.707	10	2.574	29
	7	2.709	10	2.575	29
	8	2.709	11	2.575	29
	9	2.709	7	2.606	40
	10	2.71	11	2.606	37
1 GPa	1	2.824	9	2.726	39
	2	2.83	10	2.728	41
	3	2.832	12	2.735	50
	4	2.836	8	2.744	49
	5	2.839	9	2.747	46
	6	2.84	10	2.757	46
	7	2.842	10	2.769	42
	8	2.844	11	2.769	44
	9	2.846	7	2.776	52
	10	2.849	11	2.776	52

Table S5. Calculated S_1 and T_1 excitation energies, singlet-triplet energy gap (ΔE_{ST}), and spin-orbit coupling (SOC) strength of $(TBA)_2Cu_4Br_6$ at selected pressures.

Pressure	S_1 Energy E_{S_1} (eV)	T_1 Energy E_{T_1} (eV)	Energy Gap ΔE_{ST} (eV)	Effective SOC Strength (a.u.)
1 atm	2.699	2.565	0.134	6.6551×10^{-5}
1 GPa	2.824	2.726	0.098	2.2120×10^{-4}

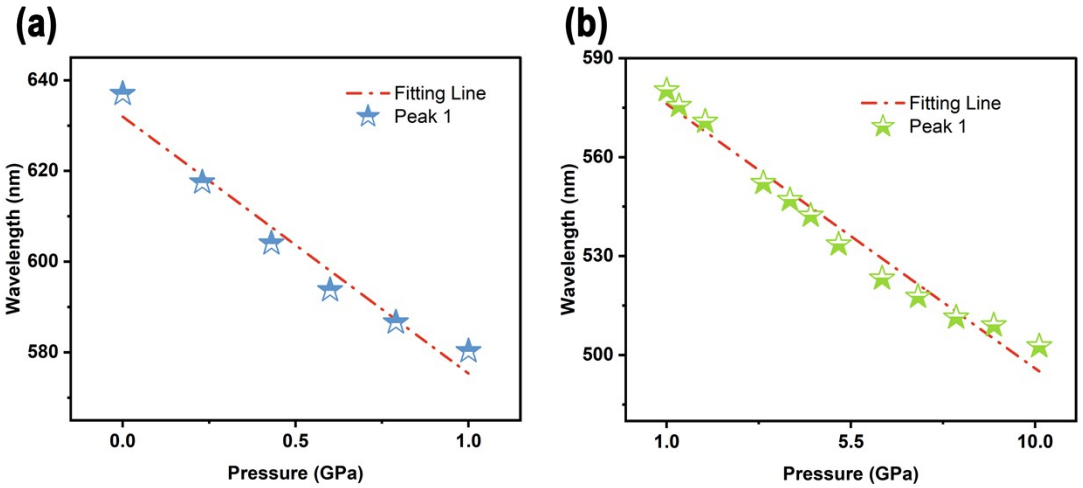

Figure S13. Pressure-dependent shift of Peak 1 during the first compression cycle. (a) Evolution of peak 1 in the 0–1 GPa range and Linear fitting results. (b) Evolution of Peak 1 position in the 1–10 GPa range and Linear fitting results.

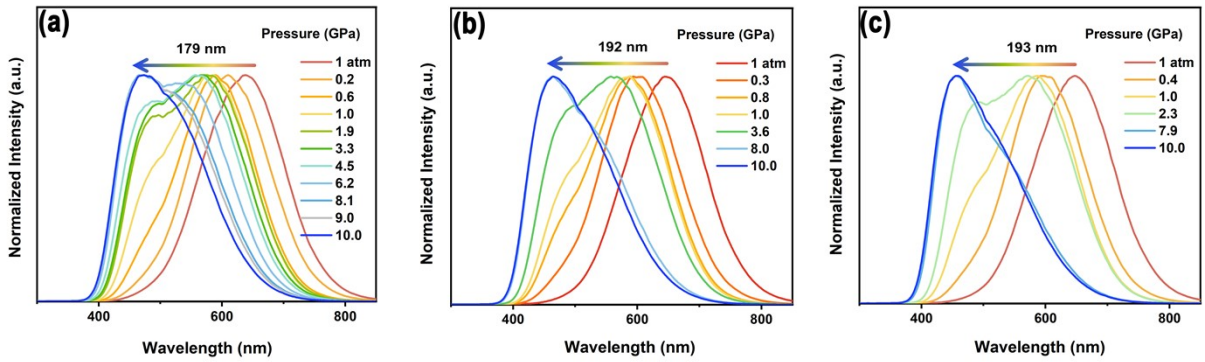

Figure S14. Normalized PL spectra during the first, second and third compression cycles (0–10 GPa). (a) First compression. (b)Second compression. (c)Third compression.

References

1. Z. Ma, Q. Li, J. Luo, S. Li, L. Sui, D. Zhao, K. Yuan, G. Xiao, J. Tang, Z. Quan and B. Zou, Journal of the American Chemical Society, 2021, 143, 15176–15184.
2. M. Cong, Q. Li, X. Wang, J. Yang, Y. Li, L. Ye, G. Xiao and B. Zou, ACS Materials Letters, 2025, 7, 996–1002.
3. A. Sillen and Y. Engelborghs, Photochemistry and Photobiology, 1998, 67, 475–486.